https://doi.org/10.5194/egusphere-2025-4099
Preprint. Discussion started: 10 September 2025

A process-informed framework linking temperature-rainfall projections and urban flood modeling

Wenyue Zou[1,2], Ruidong Li[3], Daniel B. Wright[4], Jovan Blagojevic[5], Peter Molnar[5], Mohammad A. Hussain[4], Yue Zhu[6], Yongkun Li[3,7], Guangheng Ni[3], and Nadav Peleg[1,2]

[1]Institute of Earth Surface Dynamics, University of Lausanne, Lausanne, Switzerland
[2]Expertise Center for Climate Extremes, University of Lausanne, Lausanne, Switzerland
[3]State Key Laboratory of Hydro-science and Engineering, Department of Hydraulic Engineering, Tsinghua University, Beijing, China
[4]Department of Civil and Environmental Engineering, University of Wisconsin-Madison, Madison, USA
[5]Institute of Environmental Engineering, ETH Zurich, Zurich, Switzerland
[6]Future Cities Laboratory, Singapore-ETH Centre, Singapore
[7]Beijing Water Science and Technology Institute, Beijing, China

Correspondence: Wenyue Zou (wenyue.zou@unil.ch) and Ruidong Li (lyy0744@mail.tsinghua.edu.cn)

Abstract. Predicting changes in urban pluvial flood hazards under climate warming is crucial for risk mitigation and disaster management. A key challenge in simulating future urban flood hazards is the scarcity of high-resolution rainfall projections, particularly at the sub-daily and kilometer scales required for hydrodynamic modeling. We present a cascading process-informed framework that requires minimal observed climatic data, enabling scenario analysis even in data-scarce cities. This framework consists of a distribution-based spatial quantile mapping (DSQM) method to morph observed rainfall fields conditioned on temperature changes, a stochastic storm transposition (SST) method to account for the spatial variability of urban rainfall, and a rain-on-grid hydrodynamic model (AUTOSHED) for efficient simulation of urban pluvial floods at high spatio-temporal resolution. The framework allows the generation of stochastic rainfall fields under different rainfall return levels and regional warming levels. It supports the quantification of changes in future urban flood statistics with detailed hazard maps of inundation depth, duration, and flow velocity. We select the metropolitan area of Beijing (300 km^2) as a case study area and utilize gridded hourly and 1 km rainfall data to simulate flood evolution at 5 min and 5 m resolution under regional warming levels of 1°C, 3°C, and 5°C relative to the period 1998-2019. Our results show that with rising temperatures, regional storms tend to become more intense but smaller in spatial extent, which may in turn drive increased flood depth, accelerated flow velocity, and deeper inundation, collectively elevating pluvial flood risk. Specifically, mean rainfall intensity increases by 6%, 11%, and 20% (respectively with the warming levels), peak flood depth exhibits a nonlinear increase of 4%, 7%, and 8%, due to the complex interactions of reduced storm area, increased storm intensities, and rainfall spatial variability. The proposed DSQM–SST–AUTOSHED framework offers a data-driven, physically grounded approach to assess urban flood risk under regional warming, and only requires observed rainfall fields and reanalysis temperature datasets, readily accessible from public sources, making the approach easily extendable to other cities.

https://doi.org/10.5194/egusphere-2025-4099
Preprint. Discussion started: 10 September 2025

1 Introduction

Urban pluvial floods are among the most severe climate- and water-related hazards, causing fatalities and severe economic losses worldwide (Duan et al., 2016; Rözer et al., 2021; Lehmkuhl et al., 2022; Polo-Martín, 2025). Cities can experience unusual amounts of rainfall, such as daily rainfall approaching or even exceeding their typical annual total. For example, in the urban flood that occurred in 2024 in Valencia, Spain, daily rainfall accumulated up to its annual average value (500 mm), resulting in floods that led to 200 fatalities and economic losses of approximately 480 million euros (Polo-Martín, 2025). Severe urban flooding has also been documented in China (Fu et al., 2025), Europe (Lehmkuhl et al., 2022), the United States (Saharia et al., 2017), and elsewhere.

Urban pluvial floods occur when intense rainfall over a short period generates volumes of water that exceed the capacity of the urban drainage system (Rözer et al., 2021). Under the synergistic effect of climate change and rapid urbanization, the frequency and intensity of short-duration heavy rainfall events are predicted to increase significantly, amplifying future pluvial flood risk (Wasko and Sharma, 2014; Wright et al., 2019; Fowler et al., 2021b; Peleg et al., 2025). This underscores the urgent need for robust projections of extreme rainfall and corresponding pluvial flood dynamics to inform targeted adaptation strategies and mitigate associated economic losses and societal impact. However, such projection faces several key challenges, including (i) the scarce availability of long-term high-resolution (i.e., at sub-daily and km scales) future rainfall fields (Zou et al., 2025), due to the high computational demands in convection-permitting models for simulating long-term and multiple climate scenarios; (ii) the inadequate estimation of rainfall extremes across spatial and temporal scales (Wright et al., 2020), with nonstationary change under climate warming; and (iii) lack of efficient pluvial flood simulators that can compute flow depth, velocity, and inundation duration at very high, meter-scale, resolution (Guo et al., 2021; Cache et al., 2024).

Considering the first challenge, global circulation models and regional climate models can provide long-term climate projections; however, their coarse spatial resolution ($10^1 - 10^2$ km) and absence of physically-based convective schemes limit their ability to accurately represent sub-daily rainfall extremes (Westra et al., 2014; Prein et al., 2015; Wang et al., 2024). Conversely, convection-permitting models can adequately simulate rainfall fields at $< 10^1$ km spatial resolution and sub-hourly temporal resolution (Prein et al., 2015), but their high computational cost hampers their global application, particularly for long-term simulations, large ensemble sizes, and multiple climate–emission scenarios. A computationally efficient alternative is to adjust gridded rainfall observations derived from remote sensing (such as satellites or, preferably, higher-resolution weather radars) to have rainfall characteristics matching future climate conditions. This approach remains largely underexplored; one example is the distribution-based spatial quantile mapping method (Zou et al., 2025), which projects future changes in spatiotemporal structure of rainfall fields by morphing their marginal spatial intensity distributions according to rainfall–temperature scaling relationships.

Regarding the second challenge, extreme value analysis (Katz et al., 2002) is typically used to estimate the probability that a given rainfall intensity will be exceeded within a specified return period. The corresponding results are often summarized as rainfall intensity-duration-frequency (IDF) curves (Koutsoyiannis et al., 1998), which serve as fundamental inputs for urban drainage design and flood risk management (Martel et al., 2021). However, it is widely recognized that spatial variability in

https://doi.org/10.5194/egusphere-2025-4099
Preprint. Discussion started: 10 September 2025

rainfall significantly influences the dynamics of urban pluvial floods, particularly for floods under short-duration convective storms (Fowler et al., 2021b; Peleg et al., 2022). Conventional IDF curves rely on point-scale (station-based) rainfall observations (Zou et al., 2021) and, in most cases, inadequately represent the inherent spatial variability (Wright et al., 2014a; Meng et al., 2025), even when multiple stations are considered (Peleg et al., 2018). One possible solution is utilizing stochastic storm transposition (SST) methods (Wright et al., 2017, 2020), which enable estimating rainfall extreme frequencies over arbitrary spatial scales by randomly resampling and geographically translating historical rainfall fields within a defined domain, enlarging rainfall records by incorporating nearby storms passing the region of interest (Wright et al., 2013). By introducing modified rainfall fields, consistent with climate model projections, into the SST approach, it is possible to estimate the non-stationary changes in future spatial-scale IDF curves (Zou et al., 2025).

The last challenge concerns the ability to perform efficient flood simulations while providing critical flood hazard indicators, such as inundation depth and flow velocity, at refined scales across the urban area (Rosenzweig et al., 2021). Such simulations can be physically performed using simple elevation-based models, 1D/2D dual drainage models, or full hydrodynamic models (Cea et al., 2025). The latter model type, also known as rain-on-grid models, can simulate flood dynamics by solving two-dimensional shallow water equations with spatially variable source terms that account for rainfall-runoff and sewer drainage interactions (Perrini et al., 2024a; Ming et al., 2025). These models can feature coupled hydrological and hydrodynamic processes, integrate high-resolution elevation and meteorological forcings. Yet, they involve significant trade-offs: their simulations often demand extensive computational time due to the use of highly discretized meshes required for a refined representation of heterogeneous urban surfaces. This, in turn, necessitates the development of parallel schemes based on high-performance computing techniques, such as graphical processing units (GPUs) (Costabile et al., 2023; Li et al., 2023b; Sanders et al., 2025).

Here, we propose a computationally efficient process-informed framework for projecting warming-induced urban pluvial floods by integrating recently developed methods that address the three aforementioned challenges. Our framework provides a robust, efficient, and replicable method for assessing future changes in regional storm and flood statistics, particularly in cities where high-resolution data from climate models is lacking. We first present the framework and then apply it to a medium-sized urban area of 300 km^2 in Beijing, China, as a case study. We demonstrate how observed rainfall data can be "morphed" according to projected temperature, how this affects IDF curves, and the resulting implications for urban flooding.

2 A process-informed framework for projecting future urban floods

Instead of relying on future rainfall projections from climate models, we propose a framework to project future rainfall extremes and urban flooding using only observed rainfall fields and temperature, at a resolution sufficiently high to enable urban flood simulations, as illustrated in Fig. 1.

The proposed framework is applicable under three conditions: (i) it assumes that changes in extreme short-duration rainfall are primarily driven by thermodynamic processes, rather than dynamic ones (e.g., alterations in large-scale synoptic conditions), as appears to be the case in multiple regions (Dallan et al., 2024b; Wang et al., 2024); (ii) the framework is tailored

https://doi.org/10.5194/egusphere-2025-4099
Preprint. Discussion started: 10 September 2025

for convective rainfall events, which are the predominant cause of urban pluvial flooding in many regions (Huang et al., 2022; Torelló-Sentelles et al., 2024). While the framework may also be extendable to other types of rainfall, its application to these has not yet been systematically evaluated; and (iii) the framework reproduces rainfall spatial structures by analyzing observed properties such as storm area, peak intensity, and spatial distribution. Consequently, it cannot extrapolate to generate or account for unobserved features of extreme rainfall fields (i.e., plausible extreme events that are yet unseen). Nevertheless, the stochastic space-time transposition of the storms applied in the framework is known to largely compensate for the under-representation of such unique events in the record (Wright et al., 2020).

The framework is composed of three sequential components (Fig. 1):

- First, gridded rainfall fields over a sufficiently long period with high spatio-temporal resolution (preferably 1 km and hourly or finer) need to be collected. Such data can be derived from weather radar or other remote sensing products and, if necessary, downscaled to the required resolution. Temperature data, required by rainfall–temperature scaling, may be used at coarser spatial and temporal resolutions, since only the average regional temperature over the domain at the hour of rainfall, or up to one day before rainfall initiation, is required. The Distribution-based Spatial Quantile Mapping (DSQM) is then applied to morph observed rainfall fields according to different future warming levels within the study region. Details on the rainfall–temperature scaling and DSQM methods are provided in Section 2.1.

- Second, the observed and morphed rainfall fields are used as input to an SST model (Section 2.2). By creating an archive of extreme rainfall fields and randomly transposing them elsewhere in the domain, extreme rainfall statistics can be derived for a grid cell or arbitrary area such as a watershed or neighborhood. This allows for the construction of storm return levels for both present and future regional warming levels, while accounting for natural climate variability.

- Finally, extreme storms sampled from SST for a given rainfall return period are used as input into a rain-on-grid flood model. We use a coupled hydrological-hydrodynamic model, the AUTOSHED model (Section 2.3), to compute flood hazard maps representing the spatial distribution of inundation depths and flow velocities, which can be compared between present and future rainfall extremes, under different return periods and regional warming levels.

2.1 Distribution-based spatial quantile mapping (DSQM)

The DSQM method, which morphs both the intensity and spatial structure of observed rainfall fields driven by temperature changes, is described in detail by Zou et al. (2025); only a summary of the method is provided here. At its core, DSQM modifies four key properties of rainfall fields at each time step: the mean rainfall over the entire domain, the rainfall-affected area (i.e., the rainfall spatial extent), the magnitude of the spatial variation of rainfall within the domain (i.e., the rainfall spatial coefficient of variation), and the most intense portion of rainfall (e.g., the 99th percentile) in the domain. The following steps are taken:

https://doi.org/10.5194/egusphere-2025-4099
Preprint. Discussion started: 10 September 2025

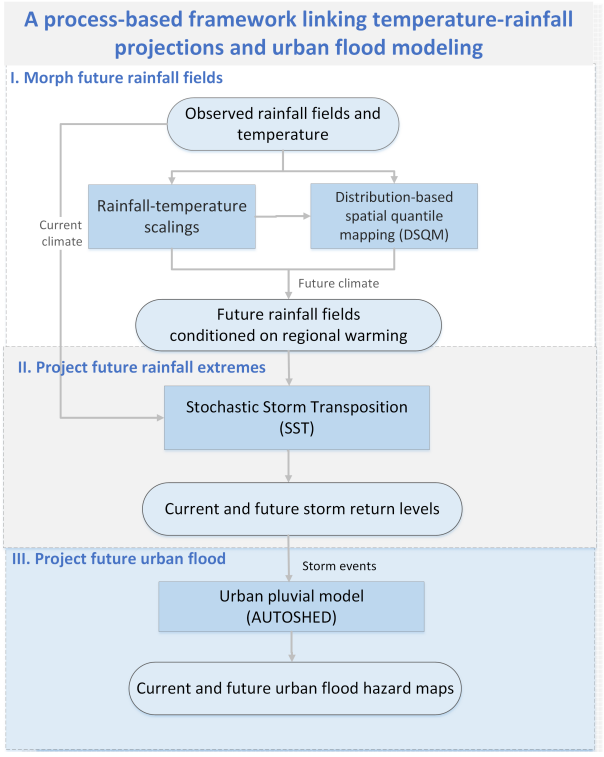

Figure 1. Schematic illustration of the process-based framework linking temperature-rainfall projections and urban flood modelling.

- The scaling relationship between rainfall and temperature is estimated using the quantile regression method (Wasko and Sharma, 2014). The scaling is first derived for the domain-averaged rainfall intensity and then extended to other rainfall properties, conditioned on its magnitude.
- The rainfall-affected area is modified. If the scaling of the rainfall area with temperature is positive, 'dry' grid cells near the 'wet' grid cells will be converted into 'wet' grids, until the desired wet area is met. If the scaling is negative, the grids with the lowest rainfall intensities will be classified as 'dry' until the quantity of the desired wet area is satisfied.
- The rainfall intensities of the new rainfall fields are transformed into quantile fields using a selected marginal distribution, such as Gamma, Weibull, or Lognormal, depending on the rainfall type and climate region.
- Finally, the quantile fields are back-transformed into new rainfall fields, basing them on the projected values of the other rainfall properties under the imposed temperature level.

An example of the method is presented in Fig.2, where an hourly rainfall field recorded over Beijing is morphed to represent a 2°C regional warming level, assuming a hypothetical 7% $°C^{-1}$ increase in mean areal rainfall intensity and a 8% $°C^{-1}$ decrease in the rainfall-affected area, demonstrating that the regional storm becomes more intense and localized with temperature warming.

https://doi.org/10.5194/egusphere-2025-4099
Preprint. Discussion started: 10 September 2025

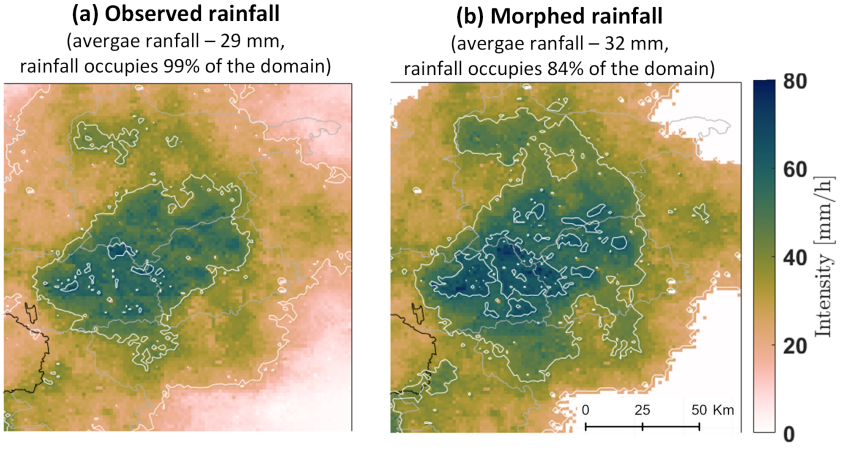

Figure 2. (a) An example of an observed rainfall field (1 h and 1 km resolution). (b) Future projected rainfall field for a 7% $^{\circ}C^{-1}$ increase in mean areal rainfall intensity and 8% $^{\circ}C^{-1}$ decrease in rainfall-affected area under 2°C regional warming.

2.2 Stochastic Storm Transposition (SST)

SST is a rainfall frequency analysis method that estimates spatially distributed rainfall extremes by resampling and transposing observed rainfall fields within a defined domain (Foufoula-Georgiou, 1989; Wilson and Foufoula-Georgiou, 1990). It enables computation of IDF curves for a given location or region while explicitly considering the rainfall spatial structure, without manipulating or interpolating observed data obtained from point sources (e.g., from multiple rain gauges; Wright et al., 2013). Furthermore, SST can produce robust rainfall frequency analysis even with relatively limited rainfall data (i.e., less than the recommended 30 years, Wright et al., 2013, 2014b), making it suitable for applications where only a few years of high-resolution gridded rainfall data from weather radar are available. The resampling and transposition of storms within the domain effectively mimic the natural spatial variability of heavy rainfall, ensuring its adequate representation in the resulting IDF curves (Wright et al., 2013). An overview of the development and applications of the SST method is provided by Wright et al. (2020).

In our framework, we have implemented the SST method through the RainyDay model (Wright et al., 2017), which follows a four-step procedure:

- First, define the area of interest (e.g., city) where rainfall IDF are to be estimated. In addition, define a transposition domain, which is a larger geographic region surrounding the area of interest and is characterized by climatology and topography similar to the area of interest, such that extreme rainfall properties are approximately homogeneous.
- Next, create a regional storm catalog from gridded rainfall observations for a given duration of interest t, by including the m storms with the largest t-duration accumulation rainfall within the area of interest.

https://doi.org/10.5194/egusphere-2025-4099
Preprint. Discussion started: 10 September 2025

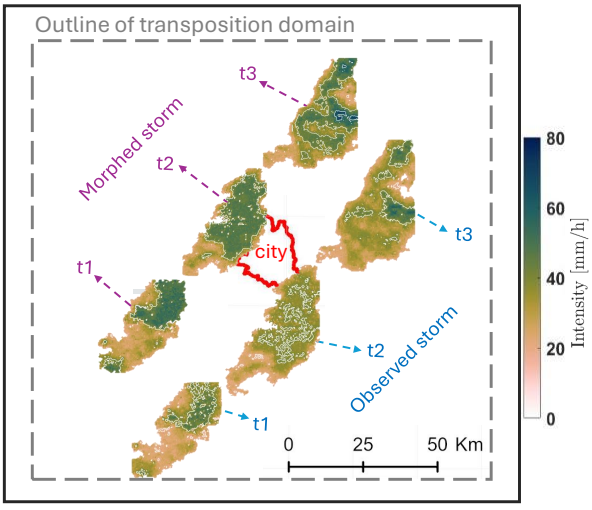

Figure 3. SST transposition domain (grey dashed box) around an interested city area (red polygon). Observed storm trajectory for a single historical storm (blue arrows), sampled here at three-hourly intervals for clarity, and DSQM-based projected future trajectory of the same storm after randomized transposition via SST (purple arrows). The transposed future storm exhibits higher mean areal rainfall intensity and spatial heterogeneity.

- Storms from the catalog are then resampled and transposed to produce multiple trajectories of extreme storms. This involves generating a random number of annual storm arrivals using the Poisson distribution or other count distribution. The transposition can be either uniform or non-uniform moving distance along east-west and north-south direction. The maximum rainfall over the area of interest is extracted from each simulated year and recorded.

- In the last step, the model assigns recurrence intervals non-parametrically by ranking the simulated annual maxima. The natural variability is derived by repeating the previous step multiple times.

The observed and DSQM-morphed storms are both used as input to the SST model. Figure 3 illustrates how the SST defines different trajectories, i.e., setting random starting positions and non-uniform movement while keeping velocity unchanged, for an observed storm from the archive corresponding to a specific rainfall return level, and for the same storm after morphing it with the DSQM (now heavier, with enhanced spatial heterogeneity).

2.3 The AUTOSHED urban pluvial flood model

Our framework employs the coupled hydrological-hydrodynamic AUTOSHED model for simulating pluvial floods (Li et al., 2023b). AUTOSHED implements the rain-on-grid approach (Hall, 2015; Perrini et al., 2024b) where surface runoff generation and routing processes are sequentially simulated on triangular-shaped meshes under spatially distributed rainfall forcings. To achieve a detailed representation of surface micro-topography, road and river boundaries are incorporated as break-lines during mesh generation (Pizzileo et al., 2024), enabling mesh edges to align adaptively with these features and accurately capture

https://doi.org/10.5194/egusphere-2025-4099
Preprint. Discussion started: 10 September 2025

their elevation profiles. At each time step, AUTOSHED first performs distributed rainfall-runoff simulations on each triangular unit. Each unit is divided into impervious and pervious parts according to the empirical impervious ratio, and AUTOSHED calculates the total surface runoff as the area-weighted sum of each component. The rainfall-runoff simulation inlcudes typical urban hydrological processes such as building interception, vegetation interception, and soil infiltration, where related parameterization details can be found in Ni et al. (2008) and Järvi et al. (2011) and in Section S1 in the Supplementary Material.

After obtaining surface runoff, AUTOSHED solves the full two-dimensional shallow water equations to simulate the flood routing process, where all boundaries are specified as open boundaries (Li et al., 2021; Luan et al., 2024). The equations are solved by the Godunov-type finite volume method (further details are discussed by Song et al., 2011). The time integration is solved by the explicit first-order scheme and an appropriate time step is dynamically adjusted by a Courant–Friedrichs–Lewy (CFL) value of 0.5 (Courant et al., 1928) to maintain numerical stability. For computational efficiency, AUTOSHED uses a multi-core parallel architecture of GPUs (Lacasta et al., 2014).

3 Case study

3.1 Case city: Beijing Municipal Administrative Center

Beijing Municipal Administrative Center (BMC, Fig. 4b) is located within the large metropolitan area of Beijing (Fig. 4a). It serves as the eastern gateway to China's national capital, where numerous local government departments have been relocated since 2015 to reduce excessive congestion in the central city. BMC's area is approximately 300 km^2 and is relatively flat with an average slope of 1.5%. It exhibits a humid continental climate, with an average annual rainfall of 536 mm and an average annual temperature of 13°C. As one of the world's largest megacities, Beijing is particularly susceptible to pluvial floods caused by extreme storms. Rainfall exceeding 70 mm h^{-1} occurred more than 82 times in the last two decades, with an increasing trend due to climate warming (Wang et al., 2020; Zou et al., 2021). Furthermore, storms are projected to become smaller and more concentrated with higher intensity in the future (Fu et al., 2018; Zou et al., 2025), increasing the probability of the occurrence of severe flood disasters. Two notable unprecedented storms were recorded in the last decade: the first one on July 21st, 2012 (areal rainfall of 215 mm in 20 h), and the second one hitting Beijing on July 31st, 2023 (331 mm in 83 hours), resulted in heavy floods and 79 and 33 deaths, with economic losses of 1.4 billion and 60 million euros, respectively (Liu et al., 2019; Li et al., 2024). These events underscore the urgent need to evaluate the future evolution of rainfall fields with the corresponding response of flood hazards to better inform disaster risk management.

Considering data, we used gridded hourly rainfall fields at 1x1 km resolution, downscaled from the 8x8 km CMORPH product for the period from 1998 to 2019 (Zou et al., 2024). Hourly and 25x25 km near-surface air temperature data for the same period were obtained from the ERA5 climate reanalysis (Hersbach et al., 2020). These datasets were used to derive the rainfall-temperature scalings and prepare the present and future rainfall archives for the SST. In addition, we collected multi-source geographical data to set up the urban pluvial flood model, including: a 0.5 m digital elevation model (Fig. 4c) that was generated from an airborne Light Detection and Ranging (LiDAR) with a sampling density of 100 points per m^2 and a mean absolute height error of 0.05 m (Fig. 4d); a 10 m land use map from the WorldCover 2021 product (Zanaga et al., 2022) (Fig.

https://doi.org/10.5194/egusphere-2025-4099
Preprint. Discussion started: 10 September 2025

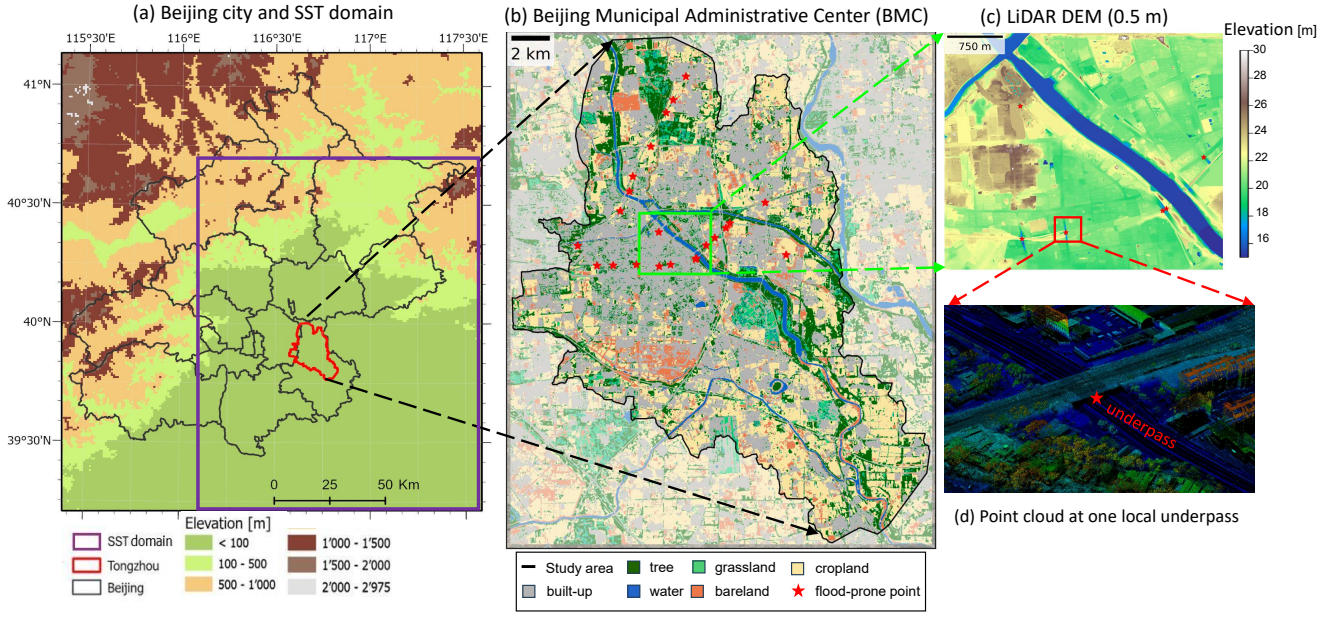

Figure 4. (a) Location map, showing Beijing Municipality area (black polygons), Beijing Municipal Administrative Center (BMC, red polygon), and the SST transposition domain (purple box). (b) Land use and historical flood-prone points within BMC. (c) Zoom in to a 0.5 m digital elevation model (DEM) in the BMC center. (d) Zoom in on a LiDAR point cloud data at a local underpass used for DEM generation.

4b), a 250 m soil hydraulic properties from the HiHydroSoil v2.0 database (Simons et al., 2020), a 250 m leaf area index data from the MODIS MOD15A2H product (Nishihama et al., 1997), and building footprint and road network layers from the Baidu map service.

Furthermore, we collected observational data related to a recent torrential rainfall event that occurred in August 2024 to evaluate the model's performance. Radar-based quantitative precipitation estimations (QPE), covering the period between 9 pm, 8th August, and 9 am, 10th August (local time), were acquired from a local agency with a spatiotemporal resolution of 500 m and 5 min (see Figure S1 in the Supplementary Material). In addition, the maximum inundation depth records at six underpasses as a result of the storm were obtained from the local agency as well.

3.2 Setting up the models

3.2.1 DSQM

To compute the rainfall-temperature scaling, we divided the hourly rainfall fields into 20 bins based on their average magnitude over the domain (to distinguish between light and heavy rain) and calculated the hourly regional average temperature across the domain for each rainfall field. We found that the scaling of the rainfall-temperature magnitude increases with the average

https://doi.org/10.5194/egusphere-2025-4099
Preprint. Discussion started: 10 September 2025

intensity of the rainfall fields, reaching a scaling of 3.6% $°C^{-1}$ as rainfall becomes heavier (see Supplementary Material Table S2 and Zou et al., 2025).

We then scaled the other rainfall properties (e.g., area and coefficient of variation) with temperature. Since these properties are conditioned on the mean rainfall over the domain, their scaling relationships were analyzed separately for each bin. We found that changes in the area of the storm as a function of temperature have an opposite signal to the storm magnitude, meaning that storms become smaller in extent (down to -2.4% $°C^{-1}$) as the rainfall magnitude increases. The spatial coefficient of variation was also found to increase with both temperature and rainfall magnitude (see Table S2 in the Supplementary Material), indicating that future extreme rainfall events will likely feature higher regional and local intensities concentrated over smaller areas.

We then applied the rainfall-temperature scaling relationships to morph the observed rainfall fields to regional warming levels of 1, 3, and 5 °C, which were subsequently used as inputs to the RainyDay model.

3.2.2 RainyDay

The transposition domain around the BMC is outlined by the purple box in Fig. 4a. It is defined based on a qualitative assessment of terrain similarity and the spatial distribution of extreme rainfall, as presented by Zou et al. (2025), to approximate homogeneous storm-occurrence across the domain.

The storm catalog for the RainyDay model was created by selecting m = 300 storms with a duration t of 72 hours that passed through the BMC region. We opted to use the Poisson resampling distribution and non-uniform transposition to shift storms within the domain stochastically; the Poisson distribution had a rate parameter of ≈13.6 storms y^{-1}, stemming from 300 storms selected from a 22-year rainfall record. Using synthetic rainfall generated by RainyDay, it first trims storms into 24-hour durations and then estimates their return levels over BMC based on 500 years of annual rainfall maxima. We ran 100 realizations (i.e., each realization contains 500 annual maxima) to provide the stochastic uncertainty corresponding to the 10- to 500-year storm return levels. The RainyDay return levels have been validated against 45 observed stations in the Beijing area, with bias less than 6% for 2- to 100-yr rainfall return levels (Supplementary Material Table S3).

For pluvial flood projection of a certain return level, we select the 50 most extreme 24-hour storm events from each return level to drive AUTOSHED for pluvial flood simulation.

3.2.3 AUTOSHED

In AUTOSHED, the BMC simulation domain is discretized into 4,055,787 triangular meshes, with a median area of 72 m^2. After mesh discretization, parameters related to rainfall-runoff generation, friction effect, and drainage capacity (Ming et al., 2025) were estimated. For rainfall-runoff simulation, we specify the empirical impervious ratio (Section 2.3) according to the land-use-based empirical values (suggested by local guidelines, BMCPNR, 2022) and assign the remaining parameters, such as soil hydraulic properties, based on geographical datasets (Section 3.1). Friction-related parameters, such as the Manning coefficients, were set to follow the aforementioned land-use-based empirical values (see Section S1 in the Supplementary Material). In the absence of a detailed sewer network in the BMC region, we parameterize drainage capacity using the road-

https://doi.org/10.5194/egusphere-2025-4099
Preprint. Discussion started: 10 September 2025

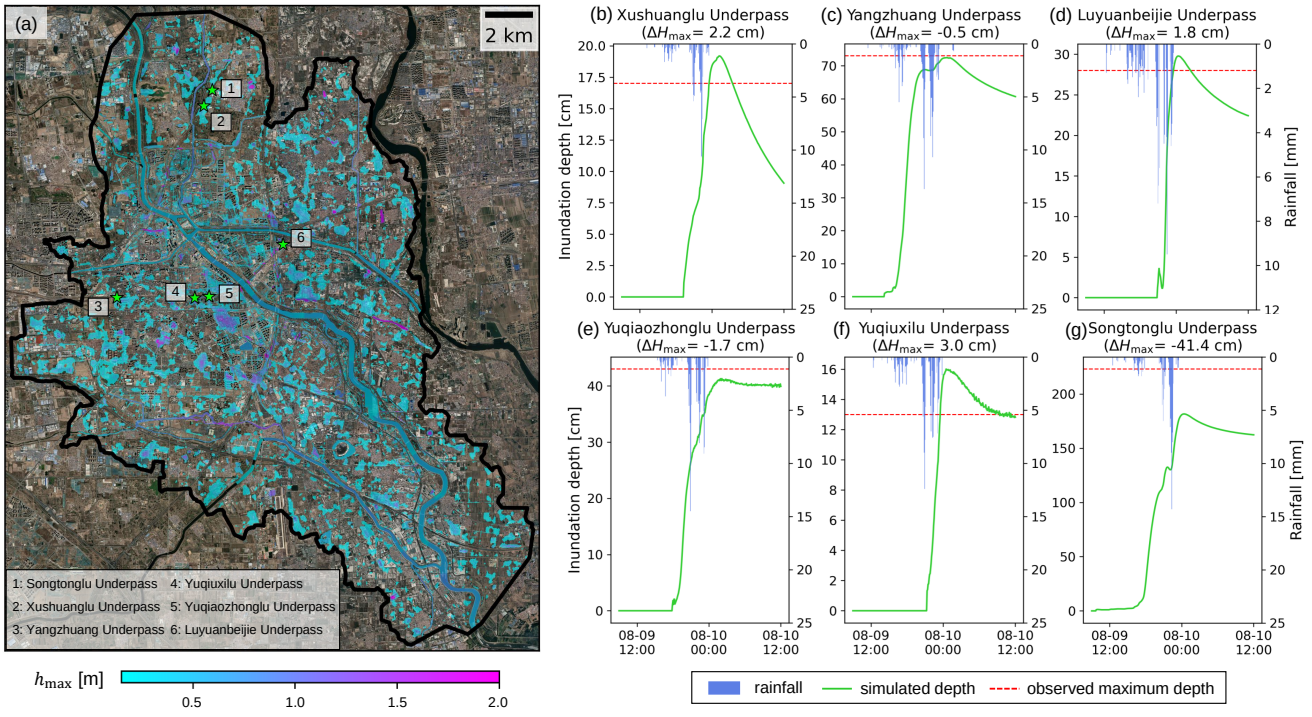

Figure 5. (a) Simulated maximum inundation depth for the August 2024 storm. (b)-(g) Simulated inundation depth compared with observed maximum inundation depth. $\Delta H_{\max}$ is defined as the simulated maximum depth minus the observed one. Basemaps are derived from ESRI World Imagery (Credit: Esri, TomTom, Garmin, FAO, NOAA, USGS, © OpenStreetMap contributors, and the GIS User Community).

drainage method (Li et al., 2023a), subtracting a uniform drainage rate of 36 mm h^{-1} from the net rainfall rate in the roadway zone only, as suggested by the Beijing Municipal Institute of City Planning and Design (Liu et al., 2022).

Based on the estimated parameters, we validate AUTOSHED using the 500 m and 5 min QPE product (Figure S1 in the Supplementary Material) and extract the simulated inundation hydrograph at six underpasses available with maximum inundation depth records (Fig.5). AUTOSHED achieves simulated absolute depth differences smaller than 5 cm at most sites, except for one underpass, for which an underestimation of 41.4 cm is observed. But this can probably be attributed to the overestimated sewer drainage in the corresponding road zones.

After the model validation, we configured AUTOSHED to run the 24-hour storms generated by the SST, using a server with an Nvidia Tesla V100 GPU (32GB) and Intel(R) Xeon(R) Gold 6226R CPU @ 2.90 GHz, for which the results are reported below. AUTOSHED can finish one 24-hour storm simulation within one hour and thus offer a very fast and efficient solution for urban pluvial flooding driven by distributed rainfall fields.

https://doi.org/10.5194/egusphere-2025-4099
Preprint. Discussion started: 10 September 2025

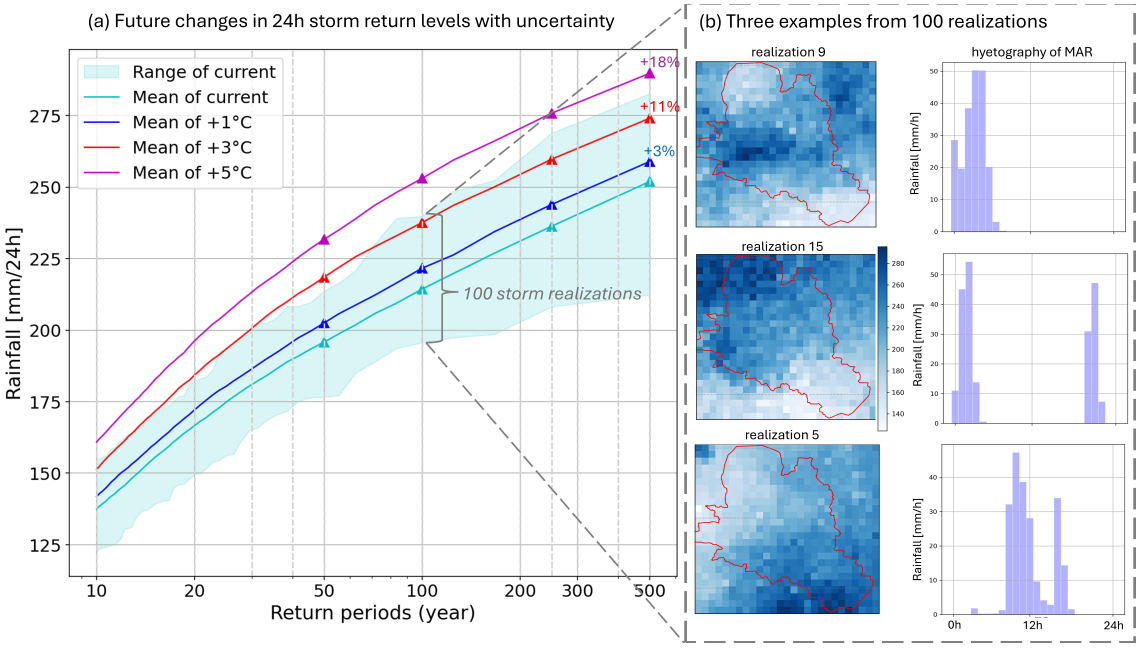

Figure 6. (a) Return levels of averaged rainfall over the BMC for 24-hour storm event and their natural variability computed from 100 realizations of storm events, (b) examples of three 24-hour storm realizations, illustrating their spatial (left column) and temporal (right column) distributions.

3.3 Future changes in regional rainfall extremes

In the following, we analyzed changes in rainfall extremes as a result of regional 1°C, 3°C, and 5°C warming in comparison with the 1998-2019 period. Projected changes in return levels of averaged rainfall over the BMC, based on 24-hour storm events, are shown in Fig. 6a. The average increase in extreme rainfall intensity for different return levels is 3%, 11%, and 18% under the 1°C, 3°C, and 5°C regional warming levels, respectively. To highlight the mean shifts in average extreme rainfall over BMC, we further computed the natural climate variability in the present climate obtained from 100 storm realizations and represent it with the green shaded area in Fig. 6a. While the mean return levels for the 1°C and 3°C warming still fall within the natural variability of the present return levels, 5°C warming is falling beyond the variability. To exemplify the high variability of the extreme rainfall both in space and time, we further illustrated three 24-hour storm events randomly selected from the simulated pool (Fig. 6b).

3.4 Future changes in urban floods

The projected changes in urban pluvial floods can be estimated from the ensemble of AUTOSHED simulations that are driven by multiple storm realizations, corresponding to different return levels and regional warming levels. Following the 100-year return level as an example, results of the current-climate simulations demonstrate that the median inundation depth, calculated

https://doi.org/10.5194/egusphere-2025-4099
Preprint. Discussion started: 10 September 2025

as the pixel-wise medians from the maximum inundation depth maps under 50 storms, is reaching up to 2 m depths within the BMC (Fig. 7a), with pronounced flooding beneath underpasses and within riparian parks in the city center (Fig. 7b). Under warming levels of 1°C, 3°C, and 5°C, median maximum flood depth increases by 4%, 7%, and 8%, respectively, while the maximum increase reaches 28% under +5°C (Fig. 7c). Fig. 7d-f illustrate the spatial distribution of median differences in inundation depths, revealing that inundation depths increase by 5-25% in both major roads and residential areas, with the most extensive impacts under +5°C extending across almost the entire urban area.

The flood inundation duration of the current climate, defined as the time during which water depth exceeds 0.4 m for the 100-year rainfall return period, is shown in Fig. 8a. The close-up to the center area (Fig. 8b) highlights the persistent water accumulation up to 12 h along major roads and in low-lying residential areas. In contrast to the distribution of the inundation depth, the distribution of the current inundation duration exhibits a more pronounced long-tail behavior, with the increase rate in maximum duration reaching 125% (Fig. 8c) for 1 °C warming. This indicates that some regions currently flooded for a short duration will face prolonged inundation under increasing temperatures. As presented in the maps in Fig. 8d-f, substantial relative changes in inundation duration can be observed at the fringes of the inundated regions. When evaluating the overall tendency, the median inundation duration increases by approximately 9%, 11%, and 8% under warming levels of 1°C, 3°C, and 5°C, respectively, indicating that further warming beyond 3°C will not necessarily result in further increases of overall inundation duration. This can be attributed to the spatiotemporal changes in extreme rainfall structures: while higher temperature raises the mean areal rainfall, it also leads to a reduction in storm area. Such localized rainfall intensification with fast movement can contribute to higher instantaneous inundation depth; however, its influence on inundation duration may be minimal or even negative due to counteracting effects between accelerated surface flow accumulation (as presented next).

We further investigated how surface flow velocities change with increasing warming. In the current climate, peak flow velocity for a 100-year return period storm generally remains below 0.5 m s^{-1} and increases up to 1 m s^{-1} along major roads and underpasses (Fig. 9a,b). Under 1°C, 3°C, and 5°C warming, the distributions of the peak flow velocities are positively skewed with medians increasing by 3% (the upper tail reaches 17%), 6% (22%), and 8% (28%), respectively (Fig. 9c). Detailed views of the center area (Fig. 9d-f) reveal considerable velocity increases (>10%) that are initially located along major roads and gradually expand into low-lying residential areas through narrow streets. Such increased velocity indicates strengthened momentum transfer and further leads to possibly faster recession and shorter inundation duration.

In summary, for major areas in the BMC, climate warming tends to intensify both inundation depth and surface flow velocity, whereas its influence on inundation duration remains limited due to counterbalancing hydrodynamic mechanisms between higher runoff volumes that are accumulating faster and subsequently leading to faster recession time.

3.5 Future changes in flood hazards

We last evaluated the impact of the changes in 100-year storms on pluvial flood hazards. Flood hazards are categorized by maximum inundation depths (following local government standards, BWA, 2025): low hazard (0.15-0.27 m), moderate hazard (0.27-0.4 m), moderate-high hazard (0.4-0.6 m), and high-hazard (>0.6 m) (Fig. 10a,b). Under current climatic conditions,

https://doi.org/10.5194/egusphere-2025-4099
Preprint. Discussion started: 10 September 2025

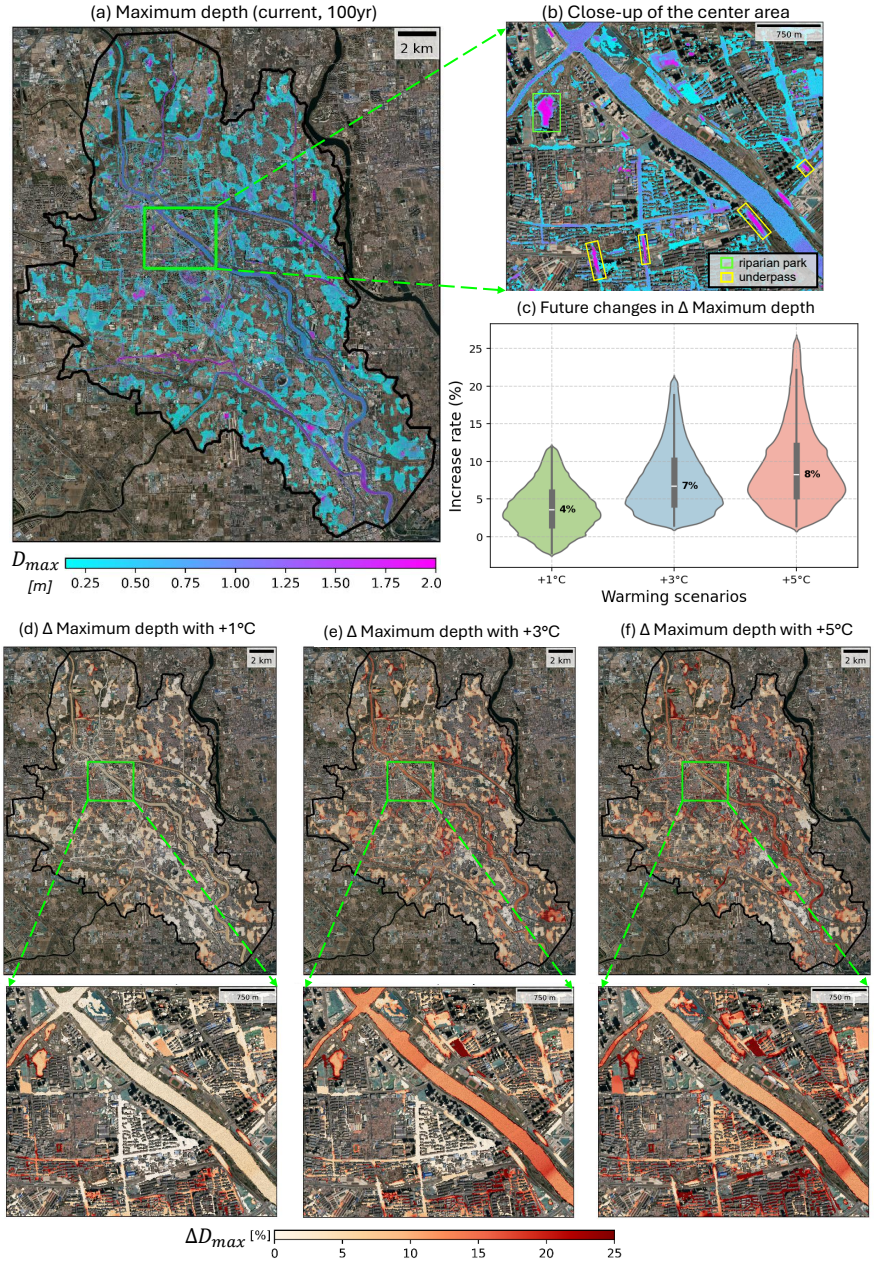

Figure 7. (a) The maximum flood depth of 100-year return level under the current climate within BMC, (b) zoom-in part in the BMC centre, (c) future changes of maximum flood depth under warming scenarios, and its spatial distribution of those changes within BMC region under 1°C (d), 3°C (e), 5°C (f) warming scenarios. Basemaps are derived from ESRI World Imagery (Credit: Esri, TomTom, Garmin, FAO, NOAA, USGS, © OpenStreetMap contributors, and the GIS User Community).

https://doi.org/10.5194/egusphere-2025-4099
Preprint. Discussion started: 10 September 2025

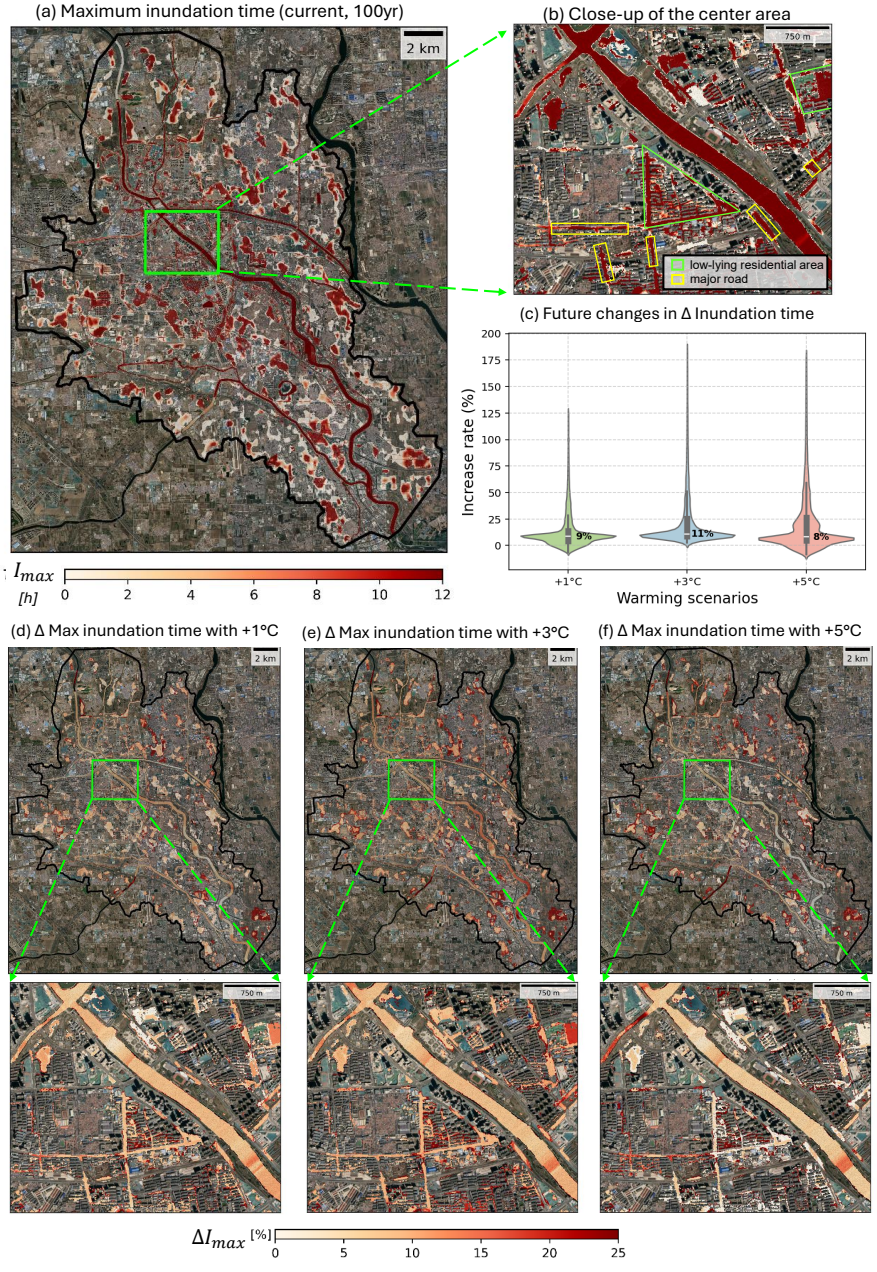

Figure 8. (a) The inundation duration for 100-year return level under the current climate within BMC, (b) zoom-in part in the BMC centre, (c) future changes of inundation duration under warming scenarios, and its spatial distribution of those changes within BMC region under 1°C (d), 3°C (e), 5°C (f) warming scenarios. Basemaps are derived from ESRI World Imagery (Credit: Esri, TomTom, Garmin, FAO, NOAA, USGS, © OpenStreetMap contributors, and the GIS User Community).

https://doi.org/10.5194/egusphere-2025-4099
Preprint. Discussion started: 10 September 2025

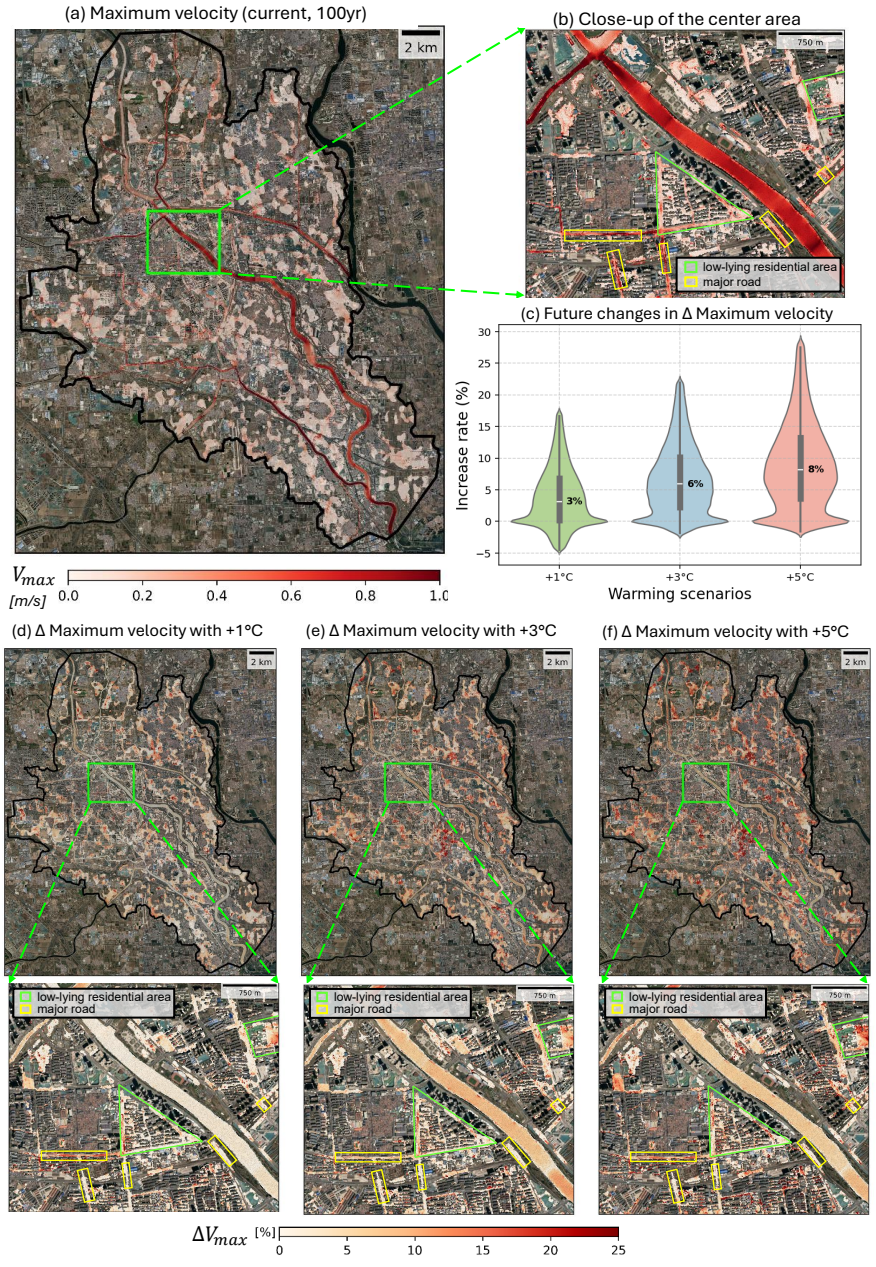

Figure 9. (a) The maximum velocity of 100-year return level for the current climate within BMC, (b) zoom-in to the BMC center, (c) future changes of maximum velocity under regional future warming levels, and its spatial distribution of those changes within BMC region under 1°C (d), 3°C (e), 5°C (f) warming level. Basemaps are derived from ESRI World Imagery (Credit: Esri, TomTom, Garmin, FAO, NOAA, USGS, © OpenStreetMap contributors, and the GIS User Community).

https://doi.org/10.5194/egusphere-2025-4099
Preprint. Discussion started: 10 September 2025

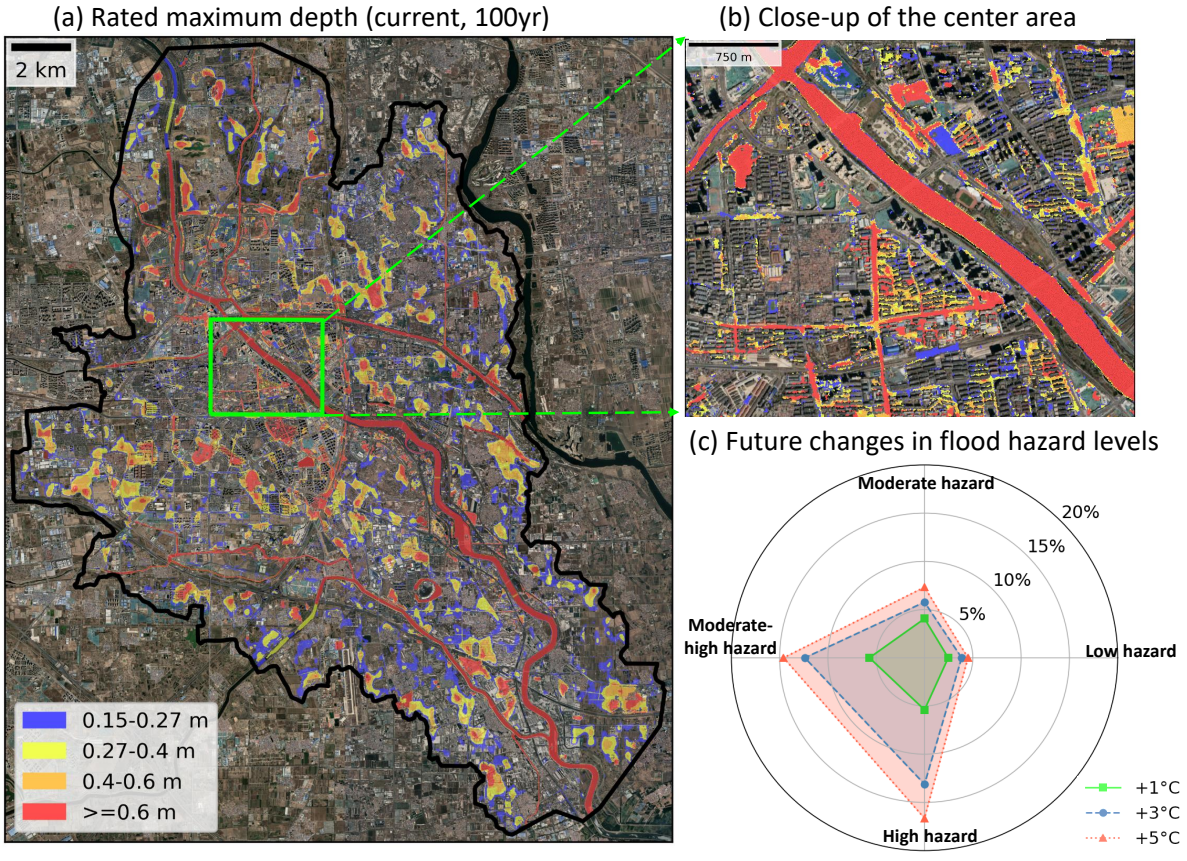

Figure 10. (a) Flood hazard for 100-yr rainfall return level under the current climate, (b) close-up of the BMC centre, and (c) changes in flood hazards assessments within BMC under different regional warming levels. Basemaps are derived from ESRI World Imagery (Credit: Esri, TomTom, Garmin, FAO, NOAA, USGS, © OpenStreetMap contributors, and the GIS User Community).

moderate-high and high hazard areas are predominantly confined to riparian parks and major roads, especially at low-lying underpasses with insufficient drainage capacities (Fig. 10b).

Analysis of the associated inundation duration (Figure S2 in the Supplementary Material) reveals that these areas can also experience long-lasting inundation for more than 12 hours, severely disrupting local transportation networks and leading to
305 substantial economic losses and potential fatalities due to the prolonged blocking of evacuation routes (Pregnolato et al., 2017). Furthermore, it should be highlighted that moderate-high and high hazard zones increase by 15-20% compared to current conditions, while low and moderate hazard areas expand by up to 5%-10% (Fig. 10c). These results demonstrate the higher sensitivity of high hazard zones to climate change, with already severely inundated areas, projected to experience more significant increases, emphasizing the urgent need for targeted adaptation measures in flood-prone locations.

https://doi.org/10.5194/egusphere-2025-4099
Preprint. Discussion started: 10 September 2025

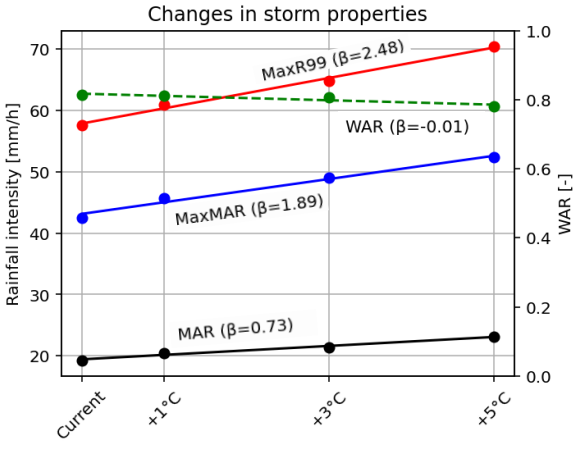

Figure 11. Future changes in mean areal rainfall (MAR, balck line), maximum mean areal rainfall ($MaxMAR$, blu line), 99th percentile of extreme rainfall at the grid-scale ($MaxR99$, red line), and area of the storm (WAR,green dash) for the 100-y storms in BMC.

4 Discussion

4.1 Changes in rainfall properties and future urban floods

One of the key strengths of the proposed framework over most existing approaches lies in its capacity to assess changes in both spatial variability and areal intensity of rainfall fields with increasing temperatures, and to evaluate their implications on urban pluvial flooding. In the BMC, for example, we examine the spatio-temporal characteristics of 50 simulated 24 h storms representing the 100-y return level under three regional warming levels. We find that while the mean rainfall over the domain is projected to increase by 0.73 mm h^{-1} $°C^{-1}$ (black lines in Fig. 11), the maximum rainfall over the domain from each 24-h storm (blue line) and the heaviest part of each storm events (i.e., the 99th percentile when analyzing the grid scale, red line) increase sharply with rates of 1.89 mm h^{-1} $°C^{-1}$ and 2.48 mm h^{-1} $°C^{-1}$, respectively. In contrast, the rainfall area exhibits a slight decline of -1% $°C^{-1}$ under regional warming levels (green dashed line in Fig. 11). The combination of higher intensities and reduced spatial coverage suggests that future storms will become more spatially concentrated, which is likely to exacerbate urban pluvial flood risks (Peleg et al., 2022; Padulano et al., 2021; Ghanghas et al., 2023). While in the BMC, the change in storm size under climate warming is relatively minor, larger negative trends have been documented elsewhere, such as the tropics (Ghanghas et al., 2023) and parts of the United States (Chang et al., 2016), which could, in some cases, reduce flood impacts as smaller storms may have a lower probability of city-wide inundation due to constrained trajectories (Chang et al., 2016). To conclude, the proposed framework provides an ideal tool to investigate flood responses to such changes in rainfall characteristics.

While rainfall was simulated at a 1 km spatial resolution, a substantially finer resolution of 5 m is adopted for the pluvial flood simulations. This raises the question of whether such refinement is warranted, given the additional computational time

https://doi.org/10.5194/egusphere-2025-4099
Preprint. Discussion started: 10 September 2025

and resources required, as well as the effort involved in obtaining a finer DEM. Hence, we further explored how sensitive the surface inundation response is to the spatial resolution of the model. We did so by selecting 22 locations that are frequently affected by flooding (see Figure S3 in the Supplementary Material) and re-running the model using the fine resolution of 5 m, and a coarser resolution of 30 and 90 m that can be obtained from multiple freely available sources (e.g., the SRTM product Werner, 2001). Across those locations, warming-driven increases in flood depth, inundation time, and velocity are markedly larger at finer grid resolutions: at 5 m resolution, increase of 1°C yields roughly 1.4 cm higher depth, 0.22 h longer inundation, and a 0.017 m s^{-1} rise in peak velocity, whereas at 30 m (90 m) these sensitivities fall to 0.4 cm (0.3 cm), 0.12 h (0.17 h), and 0.005 m s^{-1} (0.003 m s^{-1}). The reduced sensitivity at coarser spatial resolutions underscores the importance of high-resolution hydrodynamic simulations for robust assessments of urban pluvial flood risks under climate change (Xing et al., 2022; Ming et al., 2025).

Although rainfall is applied at 1 km and hourly resolutions in our case study (reflecting data availability constraints), using finer resolutions, on the order of 100 m and 5 min, is recommended for pluvial flood applications (Cristiano et al., 2017). This recommendation is due to the high spatial variability of extreme rainfall in urban environments (Maier et al., 2020; Torelló-Sentelles et al., 2024, 2025) and the rapid hydrological response characteristic of urban catchments (Cristiano et al., 2019). Such high-resolution datasets, unfortunately, remain scarce. However, the proposed framework is flexible with the resolution of rainfall fields and thus can be readily extended to finer spatial and temporal scales if relevant rainfall products are available.

4.2 Framework parameterization

Additional potential parameterizations of the framework, beyond those presented in the case study, warrant discussion. First, there is an ongoing debate regarding the appropriate approach to estimate rainfall–temperature scaling, specifically whether to use near-surface air temperature or dewpoint temperature, as the latter explicitly accounts for humidity (Lenderink et al., 2017; Ali et al., 2022). Additionally, there is discussion on whether hourly or daily temperatures better represent the atmospheric processes leading to rainfall events (Zou et al., 2024; Peleg et al., 2018b; Marra et al., 2024). While hourly near-surface air temperature is used in our case study, the framework is flexible and can be implemented with either temperature variable and at different temporal resolutions to assess the scaling.

Defining an appropriate transposition domain for the SST is critical as it influences the composition of the storm catalog and sampling of rainfall extremes. Here, we define the homogeneous transposition domain based on the similarity of the topography and rainfall extremes with the BMC area, yet different criteria, such as using the mean rainfall depth, cloud-to-ground lightning, and storm counts (Wright et al., 2013) can be applied. Further work on systematic delineation of transposition domains is underway (Benjamin et al., 2025). More importantly, instead of using a 'uniform' transposition process (Wright et al., 2014b), we have used a 'non-uniform' one in our case study, which is based on historical frequency and location of regional storms. This can be particularly relevant in urban and mountainous areas, where storm trajectories may have preferred routes (Lin et al., 2021; Medina and Houze, 2003).

https://doi.org/10.5194/egusphere-2025-4099
Preprint. Discussion started: 10 September 2025

4.3 Advantages and limitations of the framework

There are several advantages associated with the proposed framework, beyond the clear benefit of enabling application in cities lacking high-resolution rainfall data from climate models: (i) changes in rainfall properties are derived directly from the well-established thermodynamic relationship between rainfall and temperature (Trenberth et al., 2003), particularly relevant for short-duration extreme (convective) events (Lenderink et al., 2017); (ii) the framework modifies not only rainfall intensity but also the spatial coverage of storms, which can play a more significant role in urban flooding dynamics (Peleg et al., 2022); (iii) future changes are projected according to prescribed levels of regional warming (e.g., Corre et al., 2025), rather than through specific emission scenarios. This approach reduces some of the uncertainties associated with IDF projections stemming from both climate model and emission scenario discrepancies (Yu et al., 2020; Yan et al., 2021); (iv) the space-time stochasticity of extreme rainfall (also referred to as natural variability or chaotic storm evolution), which constitutes the dominant source of uncertainty in rainfall intensity–frequency relationships (Wright et al., 2020), is explicitly represented within the framework; and (v) the AUTOSHED rain-on-grid model uses GPU-accelerated ensemble hydrodynamic simulations to efficiently convert high-resolution rainfall fields into detailed flood hazard maps, including inundation and flow velocities needed for targeted disaster management (Najafi et al., 2024).

Notably, the framework primarily considers thermodynamic effects on extreme rainfall (Marra et al., 2024), but dynamic factors such as atmospheric circulation and urban areas that can affect storm frequency and intensity (Yan et al., 2021; Zhuang et al., 2024) are not explicitly taken into account. Conducting the analysis for specific rainfall types and explicitly considering their potential future frequency changes, or applying the framework to different large-scale atmospheric modes (e.g., El Niño, La Niña) and embedding their projected shifts based on information from climate models, can partially account for changes in the dynamic component. However, fully implementing the dynamic factor affecting rainfall into the framework remains a subject for future development.

We would like to note that although the proposed framework is primarily developed to address convective rainfall extremes and urban pluvial flooding, it has the potential to be used also to assess changes in urban fluvial flood hazards. A key limitation of the framework is its reliance on sampling individual extreme rainfall events rather than simulating continuous, long-term rainfall space–time series, which are often necessary for fluvial flood assessments to properly set the event's antecedent conditions (such as soil moisture content) in the hydrodynamic model. Consequently, applications to fluvial or compound pluvial–fluvial floods would require careful specification of these initial conditions.

Our proposed framework, based on open-source code and leveraging GPU-based high-performance computation techniques, offers an efficient and accessible approach for assessing future urban flood hazards. It introduces an efficient method for projecting short-duration rainfall under climate change, which is simple to implement and relies exclusively on observed rainfall and reanalysis temperature data, thus removing the dependency on high-resolution simulation results on future climatic scenarios. Applied here to the BMC region, the framework demonstrates its potential to address flood risks associated with summer convective rainfall extremes. It can be readily implemented in other urban areas where similar rainfall types contribute to plu-

https://doi.org/10.5194/egusphere-2025-4099
Preprint. Discussion started: 10 September 2025

vial flooding and should be further evaluated for its applicability to other types of extreme rainfall, although no fundamental limitations are expected.

5 Conclusions

We propose a process-informed framework to assess changes in future urban pluvial floods by using observed gridded rainfall and temperature data, without the need for climate model projections. The framework consists of three steps: (i) morphing observed rainfall fields using the DSQM method, based on observed rainfall-temperature scaling and chosen marginal distribution, to project rainfall spatiotemporal properties changes considering different regional warming levels; (ii) using the RainyDay SST approach, to obtain future changes in storms' trajectories and return levels with temperature warming; and (iii) running the AUTOSHED rain-on-grid hydrodynamic model to assess the future changes in urban pluvial flood characteristics.

As a case study, we use the framework to assess changes in pluvial floods in the Beijing Municipal Administration Center (BMC), projecting changes in urban flood depth, inundation duration, and flow velocity for different regional warming levels. We find that with rising temperatures, regional storms tend to become more intense but smaller in spatial extent. This manifests as an expansion of the inundated area, accelerated flow velocity, and increased flood depths, collectively contributing to a heightened risk of pluvial flooding. Specifically, within the BMC area, mean extreme rainfall rises by 6%, 11%, and 20% under warming levels of 1°C, 3°C, and 5°C, respectively, inducing corresponding increases of 4%, 7%, and 8% in peak flood depth.

The cascading process-based DSQM-SST-AUTOSHED framework provides a flexible, physically grounded, and replicable tool for assessing changes in urban pluvial floods considering temperature increase, with potential implications for urban planning and flood-risk adaptation. The codes for the DSQM, the RainyDay, and the AUTOSHED models are openly available and are easy to implement in other cities and climates.

Code and data availability. The code of the distributed-based spatial quantile mapping (DSQM) method, along with the 1 km x 1 km hourly rainfall data used in the Beijing case study, is openly accessible on Zenodo at https://doi.org/10.5281/zenodo.13646191. The 25 km x 25 km hourly 2-m near-surface temperatures used for the rainfall-temperature scaling were from the ERA5 climate reanalysis data and downloaded from (Hersbach et al., 2023) (last access: June 2024). The RainyDay model (Wright et al., 2017), which was used to estimate rainfall extremes via the stochastic storm transposition (SST) method, is openly available and can be downloaded via https://github.com/HydroclimateExtremesGroup/RainyDay. The AUTOSHED model prepared for one sample simulation of pluvial flood in BMC can be downloaded via https://doi.org/10.5281/zenodo.15869025 (last access: 9 August 2025). The WorldCover 2021 product for land use can be accessed from here: https://worldcover2021.esa.int/download (last access: 9 August 2025). The HiHydroSoil v2.0 product for soil hydraulic properties can be obtained from: https://www.futurewater.eu/projects/hihydrosoil/ (last access: 9 August 2025). The MODIS MOD15A2H product for leaf area index can be found in the following link: https://doi.org/10.5067/MODIS/MOD15A2H.006 (last access: 9 August 2025). Building footprint and road network data can be downloaded from:www.map.baidu.com (last access: 9 August 2025). The BMC's high-resolution LiDAR-based DEM is not publicly available.

https://doi.org/10.5194/egusphere-2025-4099
Preprint. Discussion started: 10 September 2025

Author contributions. WYZ: Conceptualization, Funding acquisition, Data curation, Formal analysis, Methodology, Software, Writing - original draft, Writing - review & editing; RDL: Conceptualization, Funding acquisition, Formal analysis, Methodology, Software, Writing - original draft, Writing - review & editing; DBW: Conceptualization, Methodology, Software; PM: Conceptualization, Writing - review & editing; JB: Writing - review & editing; AMH: Writing - review & editing; YZH: Writing - review & editing; YKL: Data acquisition; GHN: Writing - review & editing; NP: Conceptualization, Funding acquisition, Methodology, Resources, Supervision, Writing - review & editing

Competing interests. At least one of the (co-)authors is a member of the editorial board of *Hydrology and Earth System Sciences*.

Acknowledgements. GHN and RDL acknowledge the National Key Research and Development Program of China (2022YFC3090604). WZ acknowledges the support of the China Scholarship Council (CSC Grant number: 202106040028) and the Agassiz Foundation at the University of Lausanne. NP acknowledges the support of the Swiss National Science Foundation (SNSF Grant number: 194649, "Rainfall and floods in future cities"). DBW acknowledges the support of the U.S. National Science Foundation Division of Civil, Mechanical, and Manufacturing Innovation (grant number 2053358).

https://doi.org/10.5194/egusphere-2025-4099
Preprint. Discussion started: 10 September 2025

References

Ali, H., Fowler, H. J., Pritchard, D., Lenderink, G., Blenkinsop, S., and Lewis, E.: Towards quantifying the uncertainty in estimating observed scaling rates, Geophysical Research Letters, 49, e2022GL099 138, https://doi.org/10.1029/2022GL099138, 2022.

Benjamin, F., Daniel, W., Lei, Y., Alyssa, H. D., and Antonia, S.: An L-Moments-Based Hypothesis Test to Identify Homogeneous Storm Transposition Regions, Social Science Research Network, https://doi.org/10.2139/ssrn.5292988, 2025.

BMCPNR: the Technical Specification for Construction and Application of Mathematical Model of Urban Flooding Prevention and Control System, DB11/T 2074-2022, Beijing Municipal Commission of Planning and Natural Resources, Beijing, China, in Chinese, 2022.

BWA: Guidelines for the compilation of urban flood risk maps, DB11/T 2449-2025, Beijing Water Authority, Beijing, China, in Chinese, 2025.

Cache, T., Gomez, M. S., Beucler, T., Blagojevic, J., Leitao, J. P., and Peleg, N.: Enhancing generalizability of data-driven urban flood models by incorporating contextual information, Hydrology and Earth System Sciences, 28, 5443–5458, https://doi.org/10.5194/hess-28-5443-2024, 2024.

Cea, L., Sañudo, E., Montalvo, C., Farfán, J., Puertas, J., and and, P. T.: Recent advances and future challenges in urban pluvial flood modelling, Urban Water Journal, 22, 149–173, https://doi.org/10.1080/1573062X.2024.2446528, 2025.

Chang, W., Stein, M. L., Wang, J., Kotamarthi, V. R., and Moyer, E. J.: Changes in spatiotemporal precipitation patterns in changing climate conditions, Journal of Climate, 29, 8355–8376, https://doi.org/10.1175/JCLI-D-15-0844.1, 2016.

Corre, L., Ribes, A., Bernus, S., Drouin, A., Morin, S., and Soubeyroux, J.-M.: Using regional warming levels to describe future climate change for services and adaptation: Application to the French reference trajectory for adaptation, Climate Services, 38, 100 553, https://doi.org/10.1016/j.cliser.2025.100553, 2025.

Costabile, P., Costanzo, C., Kalogiros, J., and Bellos, V.: Toward Street-Level Nowcasting of Flash Floods Impacts Based on HPC Hydrodynamic Modeling at the Watershed Scale and High-Resolution Weather Radar Data, Water Resources Research, 59, e2023WR034 599, https://doi.org/10.1029/2023WR034599, e2023WR034599 2023WR034599, 2023.

Courant, R., Friedrichs, K., and Lewy, H.: Über die partiellen Differenzengleichungen der mathematischen Physik, Mathematische annalen, 100, 32–74, 1928.

Cristiano, E., ten Veldhuis, M.-C., and van de Giesen, N.: Spatial and temporal variability of rainfall and their effects on hydrological response in urban areas – a review, Hydrology and Earth System Sciences, 21, 3859–3878, https://doi.org/10.5194/hess-21-3859-2017, 2017.

Cristiano, E., ten Veldhuis, M.-c., Wright, D. B., Smith, J. A., and van de Giesen, N.: The Influence of Rainfall and Catchment Critical Scales on Urban Hydrological Response Sensitivity, Water Resources Research, 55, 3375–3390, https://doi.org/10.1029/2018WR024143, 2019.

Dallan, E., Marra, F., Fosser, G., Marani, M., and Borga, M.: Dynamical factors heavily modulate the future increase of sub-daily extreme precipitation in the alpine-mediterranean region, Earth's Future, 12, e2024EF005 185, https://doi.org/10.1029/2024EF005185, 2024b.

Duan, W., He, B., Nover, D., Fan, J., Yang, G., Chen, W., Meng, H., and Liu, C.: Floods and associated socioeconomic damages in China over the last century, Natural Hazards, 82, 401–413, https://doi.org/10.1007/s11069-016-2207-2, 2016.

Foufoula-Georgiou, E.: A probabilistic storm transposition approach for estimating exceedance probabilities of extreme precipitation depths, Water Resources Research, 25, 799–815, https://doi.org/10.1029/WR025i005p00799, 1989.

Fowler, H. J., Wasko, C., and Prein, A. F.: Intensification of short-duration rainfall extremes and implications for flood risk: Current state of the art and future directions, Philosophical Transactions of the Royal Society A, 379, 20190 541, https://doi.org/10.1098/rsta.2019.0541, 2021b.

https://doi.org/10.5194/egusphere-2025-4099
Preprint. Discussion started: 10 September 2025

Fu, C.-c., Liu, J.-h., Wang, H., Xiang, C.-y., Fu, X.-r., and Luan, Q.-h.: Urban storm flooding: Characteristics and management in Beijing, in: MATEC Web of Conferences, vol. 246, p. 01042, EDP Sciences, https://doi.org/10.1051/matecconf/201824601042, 2018.

Fu, S., Schultz, D. M., Lyu, H., Zheng, Z., and Zhang, C.: Creating a national urban flood dataset for China from news texts (2000–2022) at the county level, Hydrology and Earth System Sciences, 29, 767–783, https://doi.org/10.5194/hess-29-767-2025, 2025.

Ghanghas, A., Sharma, A., Dey, S., and Merwade, V.: How is spatial homogeneity in precipitation extremes changing globally?, Geophysical Research Letters, 50, e2023GL103 233, https://doi.org/10.1029/2023GL103233, 2023.

Guo, K., Guan, M., and Yu, D.: Urban surface water flood modelling – a comprehensive review of current models and future challenges, Hydrology and Earth System Sciences, 25, 2843–2860, https://doi.org/10.5194/hess-25-2843-2021, 2021.

Hall, J.: Direct Rainfall Flood Modelling: The Good, the Bad and the Ugly, Australasian Journal of Water Resources, 19, 74–85, https://doi.org/10.7158/13241583.2015.11465458, 2015.

Hersbach, H., Bell, B., Berrisford, P., Hirahara, S., Horányi, A., Muñoz-Sabater, J., Nicolas, J., Peubey, C., Radu, R., Schepers, D., et al.: The ERA5 global reanalysis, Quarterly journal of the royal meteorological society, 146, 1999–2049, https://doi.org/10.1002/qj.3803, 2020.

Hersbach, H., Bell, B., Berrisford, et al.: ERA5 hourly data on single levels from 1940 to present. Copernicus Climate Change Service (C3S) Climate Data Store (CDS), https://doi.org/10.24381/cds.adbb2d47, 2023.

Huang, J., Fatichi, S., Mascaro, G., Manoli, G., and Peleg, N.: Intensification of sub-daily rainfall extremes in a low-rise urban area, Urban Climate, 42, 101 124, https://doi.org/10.1016/j.uclim.2022.101124, 2022.

Järvi, L., Grimmond, C., and Christen, A.: The Surface Urban Energy and Water Balance Scheme (SUEWS): Evaluation in Los Angeles and Vancouver, Journal of Hydrology, 411, 219–237, https://doi.org/10.1016/j.jhydrol.2011.10.001, 2011.

Katz, R. W., Parlange, M. B., and Naveau, P.: Statistics of extremes in hydrology, Advances in water resources, 25, 1287–1304, https://doi.org/10.1016/S0309-1708(02)00056-8, 2002.

Koutsoyiannis, D., Kozonis, D., and Manetas, A.: A mathematical framework for studying rainfall intensity-duration-frequency relationships, Journal of hydrology, 206, 118–135, https://doi.org/10.1016/S0022-1694(98)00097-3, 1998.

Lacasta, A., Morales-Hernández, M., Murillo, J., and García-Navarro, P.: An optimized GPU implementation of a 2D free surface simulation model on unstructured meshes, Advances in Engineering Software, 78, 1–15, https://doi.org/10.1016/j.advengsoft.2014.08.007, 2014.

Lehmkuhl, F., Schüttrumpf, H., Schwarzbauer, J., Brüll, C., Dietze, M., Letmathe, P., Völker, C., and Hollert, H.: Assessment of the 2021 summer flood in Central Europe, https://doi.org/10.1186/s12302-022-00685-1, 2022.

Lenderink, G., Barbero, R., Loriaux, J., and Fowler, H.: Super-Clausius–Clapeyron scaling of extreme hourly convective precipitation and its relation to large-scale atmospheric conditions, Journal of Climate, 30, 6037–6052, https://doi.org/10.1175/JCLI-D-16-0808.1, 2017.

Li, B., Hou, J., Li, D., Yang, D., Han, H., Bi, X., Wang, X., Hinkelmann, R., and Xia, J.: Application of LiDAR UAV for High-Resolution Flood Modelling, Water Resources Management, 35, 1433–1447, https://doi.org/10.1007/s11269-021-02783-w, 2021.

Li, D., Hou, J., Shen, R., Li, B., Tong, Y., and Wang, T.: Approximation method for the sewer drainage effect for urban flood modeling in areas without drainage-pipe data, Frontiers in Environmental Science, 11, https://doi.org/10.3389/fenvs.2023.1134985, 2023a.

Li, R., Sun, T., Tian, F., and Ni, G.: AUTO-SHEDS: Automated UnsTructured urban flood Simulator using High-rEsolution DEM, in: XXVIII General Assembly of the International Union of Geodesy and Geophysics (IUGG), GFZ German Research Centre for Geosciences, https://doi.org/10.57757/IUGG23-3440, 2023b.

Li, X., Zhao, S., and Wang, D.: Roles of synoptic characteristics and microphysics processes on the heavy rain event over Beijing region during 29 July to 2 August 2023, Frontiers in Earth Science, Volume 12 - 2024, https://doi.org/10.3389/feart.2024.1394342, 2024.

https://doi.org/10.5194/egusphere-2025-4099
Preprint. Discussion started: 10 September 2025

Lin, Y., Fan, J., Jeong, J.-H., Zhang, Y., Homeyer, C. R., and Wang, J.: Urbanization-induced land and aerosol impacts on storm propagation and hail characteristics, Journal of the Atmospheric Sciences, 78, 925–947, https://doi.org/10.1175/JAS-D-20-0106.1, 2021.

Liu, J., Fu, C., Xiang, C., Wang, H., and Mei, C.: Urban Storm Flooding Management in Beijing, Urban Planning and Water-related Disaster Management, pp. 23–42, https://doi.org/10.1007/978-3-319-90173-2_3, 2019.

Liu, L., Sun, J., and Lin, B.: A large-scale waterlogging investigation in a megacity, Natural Hazards, 114, 1505–1524, https://doi.org/10.1007/s11069-022-05435-3, 2022.

Luan, G., Hou, J., Wang, T., Zhou, Q., Xu, L., Sun, J., and Wang, C.: Method for analyzing urban waterlogging mechanisms based on a 1D-2D water environment dynamic bidirectional coupling model, Journal of Environmental Management, 360, 121 024, https://doi.org/10.1016/j.jenvman.2024.121024, 2024.

Maier, R., Krebs, G., Pichler, M., Muschalla, D., and Gruber, G.: Spatial Rainfall Variability in Urban Environments—High-Density Precipitation Measurements on a City-Scale, Water, 12, https://doi.org/10.3390/w12041157, 2020.

Marra, F., Koukoula, M., Canale, A., and Peleg, N.: Predicting extreme sub-hourly precipitation intensification based on temperature shifts, Hydrology and Earth System Sciences, 28, 375–389, https://doi.org/10.5194/hess-28-375-2024, 2024.

Martel, J.-L., Brissette, F. P., Lucas-Picher, P., Troin, M., and Arsenault, R.: Climate change and rainfall intensity–duration–frequency curves: Overview of science and guidelines for adaptation, Journal of Hydrologic Engineering, 26, 03121 001, https://doi.org/10.1061/(ASCE)HE.1943-5584.0002122, 2021.

Medina, S. and Houze, R. A.: Air motions and precipitation growth in Alpine storms, Quarterly Journal of the Royal Meteorological Society: A journal of the atmospheric sciences, applied meteorology and physical oceanography, 129, 345–371, https://doi.org/10.1256/qj.02.13, 2003.

Meng, D., Liao, Y., Deng, Z., Chen, Y., Lai, C., Chen, X., and Wang, Z.: Spatially moving non-uniform rainstorms may exacerbate urban flooding disasters, Journal of Hydrology, 660, 133 374, https://doi.org/10.1016/j.jhydrol.2025.133374, 2025.

Ming, X., Liang, Q., and Jiang, J.: Large-scale high-resolution hydrodynamic modelling of urban floods: Some practical considerations, Journal of Hydro-environment Research, 59, 100 655, https://doi.org/10.1016/j.jher.2025.100655, 2025.

Najafi, H., Shrestha, P. K., Rakovec, O., Apel, H., Vorogushyn, S., Kumar, R., Thober, S., Merz, B., and Samaniego, L.: High-resolution impact-based early warning system for riverine flooding, Nature Communications, 15, 3726, 10.1038/s41467-024-48065-y, 2024.

Ni, G.-H., Liu, Z.-Y., Lei, Z.-D., Yang, D.-W., and Wang, L.: Continuous Simulation of Water and Soil Erosion in a Small Watershed of the Loess Plateau with a Distributed Model, Journal of Hydrologic Engineering, 13, 392–399, https://doi.org/10.1061/(ASCE)1084-0699(2008)13:5(392), 2008.

Nishihama, M., Wolfe, R., Solomon, D., Patt, F., Blanchette, J., Fleig, A., and Masuoka, E.: MODIS Level 1A Earth Location: Algorithm Theoretical Basis Document Version 3.0, https://doi.org/chrome-extension://efaidnbmnnnibpcajpcglclefindmkaj/https://modis.gsfc.nasa.gov/data/atbd/atbd_mod28_v3.pdf, 1997.

Padulano, R., Rianna, G., Costabile, P., Costanzo, C., Del Giudice, G., and Mercogliano, P.: Propagation of variability in climate projections within urban flood modelling: A multi-purpose impact analysis, Journal of Hydrology, 602, 126 756, https://doi.org/10.1016/j.jhydrol.2021.126756, 2021.

Peleg, N., Marra, F., Fatichi, S., Paschalis, A., Molnar, P., and Burlando, P.: Spatial variability of extreme rainfall at radar subpixel scale, Journal of Hydrology, 556, 922–933, https://doi.org/10.1016/j.jhydrol.2016.05.033, 2018.

https://doi.org/10.5194/egusphere-2025-4099
Preprint. Discussion started: 10 September 2025

Peleg, N., Marra, F., Fatichi, S., Molnar, P., Morin, E., Sharma, A., and Burlando, P.: Intensification of convective rain cells at warmer temperatures observed from high-resolution weather radar data, Journal of Hydrometeorology, 19, 715–726, https://doi.org/10.1029/2022GL099138, 2018b.

Peleg, N., Ban, N., Gibson, M. J., Chen, A. S., Paschalis, A., Burlando, P., and Leitão, J. P.: Mapping storm spatial profiles for flood impact assessments, Advances in Water Resources, 166, 104 258, https://doi.org/10.1016/j.advwatres.2022.104258, 2022.

Peleg, N., Koukoula, M., and Marra, F.: A 2°C warming can double the frequency of extreme summer downpours in the Alps, npj Climate and Atmospheric Science, 8, 216, https://doi.org/https://doi.org/10.1038/s41612-025-01081-1, 2025.

Perrini, P., Cea, L., Chiaravalloti, F., Gabriele, S., Manfreda, S., Fiorentino, M., Gioia, A., and Iacobellis, V.: A Runoff-On-Grid Approach to Embed Hydrological Processes in Shallow Water Models, Water Resources Research, 60, https://doi.org/10.1029/2023WR036421, 2024a.

Perrini, P., Cea, L., Chiaravalloti, F., Gabriele, S., Manfreda, S., Fiorentino, M., Gioia, A., and Iacobellis, V.: A Runoff-On-Grid Approach to Embed Hydrological Processes in Shallow Water Models, Water Resources Research, 60, e2023WR036 421, https://doi.org/10.1029/2023WR036421, e2023WR036421 2023WR036421, 2024b.

Pizzileo, S., Moretti, G., and Orlandini, S.: Flood plain inundation modeling with explicit description of land surface macrostructures, Advances in Water Resources, 188, 104 713, https://doi.org/10.1016/j.advwatres.2024.104713, 2024.

Polo-Martín, B.: Valencia's battle against floods: A cartographic review to assess water management strategies, Cartography, 8, 10 129, https://doi.org/10.24294/jgc10129, 2025.

Pregnolato, M., Ford, A., Wilkinson, S. M., and Dawson, R. J.: The impact of flooding on road transport: A depth-disruption function, Transportation Research Part D: Transport and Environment, 55, 67–81, https://doi.org/10.1016/j.trd.2017.06.020, 2017.

Prein, A. F., Langhans, W., Fosser, G., Ferrone, A., Ban, N., Goergen, K., Keller, M., Tölle, M., Gutjahr, O., Feser, F., et al.: A review on regional convection-permitting climate modeling: Demonstrations, prospects, and challenges, Reviews of geophysics, 53, 323–361, https://doi.org/10.1002/2014RG000475, 2015.

Rosenzweig, B. R., Herreros Cantis, P., Kim, Y., Cohn, A., Grove, K., Brock, J., Yesuf, J., Mistry, P., Welty, C., McPhearson, T., Sauer, J., and Chang, H.: The Value of Urban Flood Modeling, Earth's Future, 9, https://doi.org/10.1029/2020EF001739, 2021.

Rözer, V., Peche, A., Berkhahn, S., Feng, Y., Fuchs, L., Graf, T., Haberlandt, U., Kreibich, H., Sämann, R., Sester, M., Shehu, B., Wahl, J., and Neuweiler, I.: Impact-Based Forecasting for Pluvial Floods, Earth's Future, 9, https://doi.org/10.1029/2020EF001851, 2021.

Saharia, M., Kirstetter, P.-E., Vergara, H., Gourley, J. J., Hong, Y., and Giroud, M.: Mapping flash flood severity in the United States, Journal of Hydrometeorology, 18, 397–411, https://doi.org/10.1175/JHM-D-16-0082.1, 2017.

Sanders, B. F., Schubert, J. E., Martin, E.-M. H., Wang, S., Sukop, M. C., and Mach, K. J.: A fast flood inundation model with groundwater interactions and hydraulic structures, Advances in Water Resources, p. 105057, https://doi.org/10.1029/2024WR038847, 2025.

Simons, G., Koster, R., and Droogers, P.: Hihydrosoil v2. 0-high resolution soil maps of global hydraulic properties, FutureWater Report, https://www.futurewater.eu/projects/hihydrosoil, 2020.

Song, L., Zhou, J., Li, Q., Yang, X., and Zhang, Y.: An unstructured finite volume model for dam-break floods with wet/dry fronts over complex topography, International Journal for Numerical Methods in Fluids, 67, 960–980, https://doi.org/10.1002/fld.2397, 2011.

Torelló-Sentelles, H., Marra, F., Koukoula, M., Villarini, G., and Peleg, N.: Intensification and Changing Spatial Extent of Heavy Rainfall in Urban Areas, Earth's Future, 12, e2024EF004 505, https://doi.org/10.1029/2024EF004505, 2024.

Torelló-Sentelles, H., Villarini, G., Koukoula, M., and Peleg, N.: Impacts of urban dynamics and thermodynamics on convective rainfall across different urban forms, Urban Climate, 62, 102 499, https://doi.org/https://doi.org/10.1016/j.uclim.2025.102499, 2025.

https://doi.org/10.5194/egusphere-2025-4099
Preprint. Discussion started: 10 September 2025

Trenberth, K. E., Dai, A., Rasmussen, R. M., and Parsons, D. B.: The changing character of precipitation, Bulletin of the American Meteorological Society, 84, 1205–1218, https://doi.org/10.1175/BAMS-84-9-1205, 2003.

Wang, Y., Xie, X., Liang, S., Zhu, B., Yao, Y., Meng, S., and Lu, C.: Quantifying the response of potential flooding risk to urban growth in Beijing, Science of the total environment, 705, 135 868, https://doi.org/10.1016/j.scitotenv.2019.135868, 2020.

Wang, Y., Song, L., Shen, P., and Yang, Y.: Substantial Increase in Sub–Daily Precipitation Extremes of Flooding Season Over China, Geophysical Research Letters, 51, e2024GL112 182, https://doi.org/10.1029/2024GL112182, e2024GL112182 2024GL112182, 2024.

Wasko, C. and Sharma, A.: Quantile regression for investigating scaling of extreme precipitation with temperature, Water Resources Research, 50, 3608–3614, https://doi.org/10.1002/2013WR015194, 2014.

Werner, M.: Shuttle radar topography mission (SRTM) mission overview, Frequenz, 55, 75–79, https://doi.org/https://doi.org/10.1515/FREQ.2001.55.3-4.75, 2001.

Westra, S., Fowler, H. J., Evans, J. P., Alexander, L. V., Berg, P., Johnson, F., Kendon, E. J., Lenderink, G., and Roberts, N.: Future changes to the intensity and frequency of short-duration extreme rainfall, Reviews of Geophysics, 52, 522–555, https://doi.org/10.1002/2014RG000464, 2014.

Wilson, L. L. and Foufoula-Georgiou, E.: Regional rainfall frequency analysis via stochastic storm transposition, Journal of Hydraulic Engineering, 116, 859–880, https://doi.org/10.1061/(ASCE)0733-9429(1990)116:7(859), 1990.

Wright, D. B., Smith, J. A., Villarini, G., and Baeck, M. L.: Estimating the frequency of extreme rainfall using weather radar and stochastic storm transposition, Journal of hydrology, 488, 150–165, https://doi.org/10.1016/j.jhydrol.2013.03.003, 2013.

Wright, D. B., Smith, J. A., and Baeck, M. L.: Critical examination of area reduction factors, Journal of Hydrologic Engineering, 19, 769–776, https://doi.org/10.1061/(ASCE)HE.1943-5584.0000855, 2014a.

Wright, D. B., Smith, J. A., and Baeck, M. L.: Flood frequency analysis using radar rainfall fields and stochastic storm transposition, Water Resources Research, 50, 1592–1615, https://doi.org/10.1002/2013WR014224, 2014b.

Wright, D. B., Mantilla, R., and Peters-Lidard, C. D.: A remote sensing-based tool for assessing rainfall-driven hazards, Environmental modelling & software, 90, 34–54, https://doi.org/10.1016/j.envsoft.2016.12.006, 2017.

Wright, D. B., Bosma, C. D., and Lopez-Cantu, T.: US hydrologic design standards insufficient due to large increases in frequency of rainfall extremes, Geophysical Research Letters, 46, 8144–8153, https://doi.org/10.1029/2019GL083235, 2019.

Wright, D. B., Yu, G., and England, J. F.: Six decades of rainfall and flood frequency analysis using stochastic storm transposition: Review, progress, and prospects, Journal of Hydrology, 585, 124 816, https://doi.org/10.1002/2013WR014224, 2020.

Xing, Y., Chen, H., Liang, Q., and Ma, X.: Improving the performance of city-scale hydrodynamic flood modelling through a GIS-based DEM correction method, Natural Hazards, 112, 2313–2335, https://doi.org/10.1007/s11069-022-05267-1, 2022.

Yan, L., Xiong, L., Jiang, C., Zhang, M., Wang, D., and Xu, C.-Y.: Updating intensity–duration–frequency curves for urban infrastructure design under a changing environment, Wiley Interdisciplinary Reviews: Water, 8, e1519, https://doi.org/10.1002/wat2.1519, 2021.

Yu, G., Wright, D. B., and Li, Z.: The upper tail of precipitation in convection-permitting regional climate models and their utility in nonstationary rainfall and flood frequency analysis, Earth's Future, 8, https://doi.org/10.1029/2020EF001613, 2020.

Zanaga, D., Van De Kerchove, Ruben andDaems, D., De Keersmaecker, W., Brockmann, C., Kirches, G., Wevers, J., Cartus, O., Santoro, M., Fritz, S., Lesiv, M., Herold, M., Tsendbazar, N.-E., Xu, P., Ramoino, F., and Arino, O.: ESA WorldCover 10 m 2021 v200, https://doi.org/10.5281/zenodo.7254221, 2022.

Zhuang, Q., Koukoula, M., Liu, S., Zhou, Z., Gao, L., and Peleg, N.: Contradictory influences of urbanization on intense convective rainfall in a subtropical city, Environmental Research Letters, 19, 104 020, https://doi.org/10.1088/1748-9326/ad7277, 2024.

https://doi.org/10.5194/egusphere-2025-4099
Preprint. Discussion started: 10 September 2025

Zou, W., Hu, G., Wiersma, P., Yin, S., Xiao, Y., Mariethoz, G., and Peleg, N.: Multiple-point geostatistics-based spatial downscaling of heavy rainfall fields, Journal of Hydrology, 632, 130 899, https://doi.org/10.1016/j.jhydrol.2024.130899, 2024.

Zou, W., Wright, D. B., and Peleg, N.: Morphing sub-daily rainfall fields based on temperature shifts to project future changes in rainfall extremes, Water Resources Research, 61, e2024WR038 847, https://doi.org/10.1029/2024WR038847, 2025.

Zou, W.-y., Yin, S.-q., and Wang, W.-t.: Spatial interpolation of the extreme hourly precipitation at different return levels in the Haihe River basin, Journal of Hydrology, 598, 126 273, https://doi.org/10.1016/j.jhydrol.2021.126273, 2021.